Materials Research Proceedings **25** (2023) 133-140 https://doi.org/10.21741/9781644902417-17

# Influence of plastic orthotropy on clinching of sheet metal

Johannes Friedlein[1,a*], Christian Bielak[2,b], Max Böhnke[2,c], Mathias Bobbert[2,d], Gerson Meschut[2,e], Julia Mergheim[1,f] and Paul Steinmann[1,g]

[1]Institute of Applied Mechanics, Friedrich-Alexander-Universität Erlangen-Nürnberg, Egerlandstrasse 5, 91058 Erlangen, Germany

[2]Laboratory for Material and Joining Technology (LWF), Paderborn University, Pohlweg 47-49, 33098 Paderborn, Germany

[a]johannes.friedlein@fau.de, [b]christian.bielak@lwf.upb.de, [c]max.boehnke@lwf.upb.de, [d]mathias.bobbert@lwf.upb.de, [e]meschut@lwf.upb.de, [f]julia.mergheim@fau.de, [g]paul.steinmann@fau.de

**Keywords:** Anisotropy, Modelling, Clinching

**Abstract.** Clinching is a versatile mechanical joining method for assembling different sheet metal materials without auxiliary elements in short process times. The joint strength, however, solely relies on the material condition and its targeted interlock formation. Therefore, accurate material models are necessary incorporating all relevant phenomena to reliably predict the material behaviour. We extend a finite elastoplastic material model by incorporating the plastic orthotropy of the sheet metal in the joining process simulation. The anisotropy is captured by different variants of the 3D Hill 1948 yield function with associative and non-associative plastic flow. The constitutive models and the 3D clinching simulation are outlined and utilised to study the influence of plastic orthotropy focusing on the aluminium alloy EN AW-6014.

## Introduction

Clinching is a mechanical joining technique for assembling different sheet metal materials by solely cold forming the material. Thus, it does not require auxiliary parts and hole pre-alignment. However, consequently the joint strength solely relies on the sheets and the sufficient formation of an interlock during the clinch joining process. Numerical investigations are essential for the development of the process route, to gain a deeper insight and for future optimisation. This requires highly accurate and robust material models to capture the large plastic deformations [1,2] and the complex non-proportional material flow. Especially the latter could change systematically due to anisotropic plastic flow, which can be accurately captured, for instance, by the r-values. Thus, this study focuses on the inherent plastic orthotropy of the metal sheets to be joined and its influence on the joint forming.

In [3] clinched joints of differently coated thin steel sheets H180Y exhibiting high Lankford (r-) values (1.4 ... 2.0) were studied. By using an anisotropic Hill yield locus for plasticity in ABAQUS for the quasi-static loading of the clinched joint, they showed a notable influence of anisotropy on the predicted shear strength. On the other hand, in [4] only a marginal effect of the plastic orthotropy for mild deep drawing steel DC05 on the strength of the joint was observed. Therein, the anisotropic plasticity model by Hill (1948, "Hill48") [5] was used under plane stress condition and equipped with parameters also determined from Lankford values. In addition to a von Mises and plane stress Hill48 yield function, [6] utilised the more advanced anisotropy model Yld2000-2d. They investigated equivalent models for clinched joints of deep-drawing-quality steel sheet proving a significant effect of the anisotropy on the calibration. In contrast, to the previous works studying the clinched joint, for instance [7] considers the preceding clinch joining process. Therein, only a minor influence of plastic orthotropy on the interlock was shown for DC05. For a

dual-phase steel DP600 only a negligible effect of the planar anisotropy on the sheet contours after joining was found [8].

We focus on an aluminium alloy EN AW-6014 T4 with sheet thickness 2 mm. Its plastic orthotropy has already been characterised in [9] – by uniaxial tension tests and layer compression tests – being more pronounced than for a dual-phase steel HCT590X. Moreover, in contrast to the steel, the biaxial r-value of the aluminium alloy was less than 1, possibly rendering a different behaviour. The anisotropy is described by different variants of the Hill48 model including associative and non-associative flow rules. For the numerical investigations, a 3D clinching process model [10] is used. Moreover, in contrast to the state of the art, we focus on the importance of using 3D orthotropic plasticity to also capture the inherent difference between in-plane and out-of-plane plastic yielding and flow. This forms the basis to study the influence of plastic orthotropy on geometric and process-related parameters of clinch joining based on a flexible but still comparable group of anisotropy models.

## Material Modelling

Clinching involves large plastic strains modelled herein by finite plasticity based on the logarithmic strain space [11]. After a short introduction into the framework and the elasto-plasticity model, the anisotropy formulations are introduced to describe the sheet metal.

Kinematics. The deformation of the body is captured by the deformation gradient $\boldsymbol{F} = \boldsymbol{I} + \nabla_{\boldsymbol{X}}\boldsymbol{u}$ based on the unit tensor $\boldsymbol{I}$ and the gradient of the displacements $\boldsymbol{u}$. From the deformation gradient $\boldsymbol{F}$, the right Cauchy-Green strain tensor is defined as $\boldsymbol{C} = \boldsymbol{F}^T \cdot \boldsymbol{F}$.

Logarithmic strain space. As part of Seth-Hill's family of generalised strain measure, the logarithmic (Hencky) strain $\boldsymbol{H}$ is used within the logarithmic strain space and computed from the right Cauchy-Green strain tensor [11]. Due to the properties of the Hencky strain, the additive split $\boldsymbol{H} = \boldsymbol{H}^{\mathrm{e}} + \boldsymbol{H}^{\mathrm{p}}$ of the total strain into elastic and plastic part is applicable. Plasticity is herein based on a free energy density quadratic in the elastic strains $\boldsymbol{H}^{\mathrm{e}}$. Nonlinear isotropic hardening is described by a plastic potential, which is here defined by a tabular flow stress $\sigma_{\mathrm{f}}(H^{\mathrm{p,acc}})$, with the accumulated plastic strain $H^{\mathrm{p,acc}}$. The logarithmic stress tensor $\boldsymbol{T}$ is computed from the total Hencky strain $\boldsymbol{H}$ and total plastic Hencky strain $\boldsymbol{H}^{\mathrm{p}}$.

Isotropic and anisotropic yield functions. Plastic anisotropy is introduced by the classical 3D Hill48 anisotropic yield function [5] written in tensor notation [11] as

$$\Phi(\boldsymbol{T}, H^{\mathrm{p,acc}}) = \|\boldsymbol{T}\|_{\mathcal{H}_s} - \sqrt{\boldsymbol{2/3}}\ \sigma_{\mathrm{f}}(H^{\mathrm{p,acc}}) \leq 0 \quad \text{with } \|(\cdot)\|_{\mathcal{H}_s} \equiv \sqrt{(\cdot):\boldsymbol{\mathcal{H}_s}:(\cdot)} \tag{1}$$

This yield criteria is similar to isotropic von Mises (J2-) plasticity besides the generalisation of the stress norm using the deviatoric fourth order Hill tensor $\mathcal{H}_s$. Thus, for $\mathcal{H}_s = \mathfrak{I}^{\mathrm{dev}}$ (deviatoric fourth order unit tensor), we recover isotropic von Mises plasticity. The tensor $\mathcal{H}_s$ is set up from the Hill coefficients $h_{\alpha\beta}$ as described in [9, 11].

Evolution equations and algorithmic implementation. Starting from the yield condition in Eq. (1), the evolution equations are derived. This includes the symmetric plastic strain tensor $\boldsymbol{H}^{\mathrm{p}}$ and the accumulated plastic strain $H^{\mathrm{p,acc}}$ as

$$\dot{\boldsymbol{H}}^{\mathrm{p}} = \dot{\gamma}\boldsymbol{N} \quad \text{with } \boldsymbol{N}(\boldsymbol{T}) \equiv \frac{\boldsymbol{\mathcal{H}_r}:\boldsymbol{T}}{\|\boldsymbol{T}\|_{\mathcal{H}_r}}\ ; \quad \dot{H}^{\mathrm{p,acc}} = \sqrt{\boldsymbol{2/3}}\,\dot{\gamma} \tag{2}$$

based on the Lagrange multiplier $\dot{\gamma}$. The latter relation for the accumulated plastic strain is – for the non-associative model – an assumption proposed in [12], made for simplicity. Here, we have already generalised the relation for the plastic strain to incorporate a non-associative flow rule by introducing the Hill48-type tensor $\boldsymbol{\mathcal{H}_r}$. The special case of associative plasticity is recovered for $\boldsymbol{\mathcal{H}_s} = \boldsymbol{\mathcal{H}_r}$. To satisfy the yield condition also for a non-associative flow rule, we use a closest-point projection algorithm [13]. The implementation is carried out as an implicit user-defined material model in the commercial FEM-software LS-DYNA.

In this framework we identify four groups of material models that will be compared in the results section, namely isotropic plasticity "von Mises" ($\boldsymbol{\mathcal{H}_s = \mathcal{H}_r = \mathfrak{I}^{dev}}$), associative anisotropic Hill48 plasticity ($\boldsymbol{\mathcal{H}_s = \mathcal{H}_r}$) either based on r-values "Hill48-r/Hill48-rn" *or* yield stress ratios "Hill48-s", and non-associative anisotropic Hill48 plasticity identified based on r-values *and* yield stress ratios "Hill48-rs" ($\boldsymbol{\mathcal{H}_s \neq \mathcal{H}_r}$). All these models share a common basis, which is beneficial for the comparison as differences can thus be clearly attributed generating insightful cause-effect relations. Here, non-associative flow is crucial to simultaneously capture the r-values and yield stress ratios, while still being comparable to the associative basis.

**Parameter Identification**

In the following, we first briefly outline the experimental setups and results. Secondly, the computation of the anisotropy coefficients for the different models is described in detail.

Layer compression test. This test is an adaption of the conventional compression test based on DIN 50106 (see e. g. [9] for details and further literature). With this setup the plastic flow curve up to true plastic strains of about 0.7. This data is taken from [2], where a good correlation for the application in clinching process simulations was achieved with this setup. However, it needs to be kept in mind that the sheet is loaded in thickness direction, therefore we obtain the flow stress in sheet normal direction, which is thus herein chosen as reference direction. This flow stress might differ from the rolling direction due to plastic anisotropy.

Tensile tests with different sheet orientations. Tensile tests were carried out in [9] according to DIN 6892-1. To investigate the anisotropy of the aluminium sheet metal, specimens were extracted under 0°, 45° and 90° to the rolling direction (RD) by laser cutting.

Firstly, from the tensile test the r-values $r_\theta$ can be determined from the strains measured by an optical measuring system. These were evaluated at an elongation of 10 mm (20% strain), compare [9], and are $r_{0°} = 0.8060$, $r_{45°} = 0.4637$ and $r_{90°} = 0.6105$. Moreover, it is possible to compute the average or normal anisotropy $r_\mathrm{n} = [r_{0°} + 2\,r_{45°} + r_{90°}]/4 \approx 0.5860$ from these r-values [14]. This r-value is the basis for the Hill48-rn model, which corresponds to an isotropic in-plane behaviour. Here, anisotropy only affects the thickness direction, so with only one preferred direction (transverse isotropy). Thus, Hill48-rn could be solved using a 2D axisymmetric model saving computation time but still capturing the anisotropy in thickness direction. Nevertheless, for comparability the 3D simulation model was utilised.

Secondly, the yield stress ratios $\sigma_{\mathrm{yield},\theta}/\sigma_{\mathrm{yield},0°}$ $(0°: 1;\ 45°: 0.9820;\ 90°: 0.9655)$ are determined from the true stress-strain curves based on the force-elongation curves in the different sheet orientations. Here, the reference yield stress $\sigma_{\mathrm{yield},0°}$ corresponds to the rolling direction. However, our reference flow stress stems from the layer compression test and thus is determined in sheet thickness direction with $\sigma_{\mathrm{yield,thickness}}$. Therefore, the yield stress ratio $s_\theta = \sigma_{\mathrm{yield},\theta}/\sigma_{\mathrm{yield,thickness}}$ is defined. To remain consistent with the Hill48 model

$$\frac{\sigma_{\mathrm{yield,thickness}}}{\sigma_{\mathrm{yield},0°}} = \left[-1 + \frac{2}{1 + r_{0°}} + \left[\frac{\sigma_{\mathrm{yield},90°}}{\sigma_{\mathrm{yield},0°}}\right]^{-2}\right]^{-0.5} \approx 0.9205 \tag{3}$$

is computed based on [15] to transform the ratios $\sigma_{\mathrm{yield},\theta}/\sigma_{\mathrm{yield},0°}$ (with $h_{11} = 1$) to $s_\theta$ $(h_{33} = 1;\ 0°: 1.0864;\ 45°: 1.0668;\ 90°: 1.0489)$. In doing so, we further ensure that at least the r-value in RD $r_{0°}$ is exactly obtained by the Hill48-s model [16], see Fig. 1. Even though this alters the actual yield stress ratios, it is nevertheless regarded as sufficient for a fundamental study on the influence of plastic orthotropy on clinching and further improves the comparability to the isotropic von Mises model.

Anisotropy coefficients. We choose the sheet thickness direction as reference direction to be able to directly utilise the flow curve from the layer compression test as flow stress $\sigma_\mathrm{f}(H^{\mathrm{p,acc}})$. For the Hill48 anisotropy model this corresponds to the definition $(h_{33} = 1) \simeq (F_{yz} + G_{zx} = 1)$.

Moreover, we assume the out-of-plane anisotropy coefficients $h_{23}$ and $h_{31}$ to be identical to the isotropic case. From the r-values and yield stress ratios, the remaining anisotropy coefficients $h_{\alpha\beta}$ can be determined. The classical associative Hill48 anisotropic plasticity model can either solely be based on the r-values as Hill48-r/-rn models or be based on the yield stress ratios as Hill48-s model.

Hill48-r. Transforming the definitions given in [9,16], the Hill-coefficients are computed from the r-values for $h^r_{33} = 1$ as

$$h^r_{11} = \sqrt{\frac{r_{0°} + r_{90°}}{r_{90°}[r_{0°} + 1]}} \qquad h^r_{22} = \sqrt{\frac{r_{0°} + r_{90°}}{r_{0°}[r_{90°} + 1]}} \qquad h^r_{33} \equiv 1$$
$$h^r_{12} = [2r_{45°} + 1]^{-0.5} \qquad h^r_{23} = h^r_{31} = 1/\sqrt{3} \tag{4}$$

Hill48-rn. Eq. **(4)** is also applicable for the Hill48-rn model replacing $r_{0°}$, $r_{45°}$ and $r_{90°}$ by $r_{\mathrm{n}}$.

Hill48-s. From the relation between the yield stress ratios and the anisotropy coefficients for Hill48 [15] with the assumption that $h^s_{33} = 1$, the following equations result

$$h^s_{11} = s_{0°} \qquad h^s_{22} = s_{90°} \qquad h^s_{33} \equiv 1$$
$$h^s_{12} = s_{45°}\,[4 - [s_{45°}]^2]^{-0.5} \qquad h^s_{23} = h^s_{31} = 1/\sqrt{3} \tag{5}$$

The resulting Hill anisotropy coefficients $(\boldsymbol{h_{11}}; \boldsymbol{h_{22}}; \boldsymbol{h_{12}})$ with $h_{33} = 1$ and $\boldsymbol{h_{23}} = \boldsymbol{h_{31}} = 0.5774$ are for Hill48-r (1.1335; 1.0446; 0.7203), Hill48-rn (1.1230; 1.1230; 0.6785) and Hill48-s (1.0864; 1.0489; 0.6306). Hill48-rs combines the parameters from Hill48-r and Hill48-s, thus utilises two sets of Hill-coefficients. As well-known, Hill48 anisotropy can typically not simultaneously capture the experimental r-values and yield stress ratios (marked by x) [14], as shown in Fig. 1. In contrast, the non-associative Hill48-rs model combines both sets and thus describes both well. Hill48-rn (dash-dotted) captures none of the in-plane ratios exactly, but only the (not shown) thickness direction.

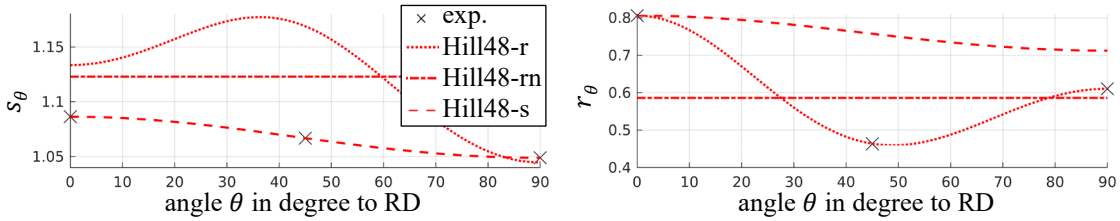


*Fig. 1. Yield stress ratios $s_\theta$ (left) and r-values $r_\theta$ (right) as function of the angle $\theta$ to the rolling direction (RD). Hill48-s (dashed) captures the experimental yield stress ratios (marked by x) precisely, but not the r-values. In contrast, Hill48-r (dotted) only captures the r-values exactly. The ratios for Hill48-rn (dash-dotted) do not depend on the in-plane orientation, but nevertheless reproduce r-values and yield stress ratios different from* 1.

**3D Clinching with Isotropic and Anisotropic Plasticity**

Subsequently, the 3D clinching process model is introduced followed by the numerical results.

3D clinching model. The 3D clinching process model and the essential settings are shown in Fig. 2 based on the validated model from [10]. To keep the meshes symmetric and be able to account all asymmetries to the influence of plastic orthotropy, eight-node hexahedral elements (ELFORM=1) without remeshing were chosen. Nevertheless, especially due to the complicated contact states, some asymmetry can result from the numerical model. Thus, all results are averaged by using the x-direction as RD and separately solving the model for RD along the y-direction (90° rotated) to account for the mentioned numerical asymmetries. The differences between the results are indicated by error bars in Fig. 5. Even though the values might scatter, the

shown ratios and trends between rolling (RD) and transverse direction (TD) were consistent for all models.

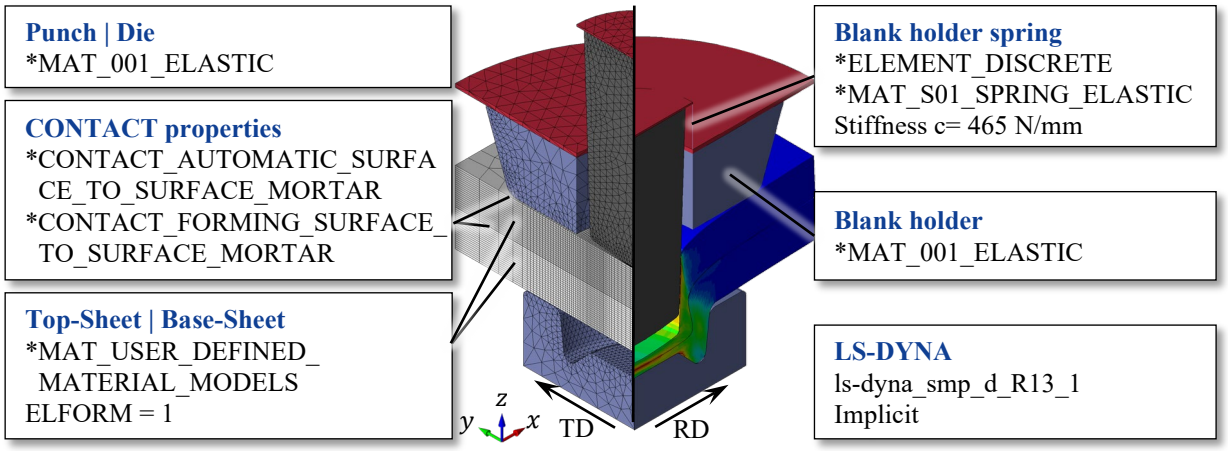


*Fig. 2. 3D clinching process model and essential simulation settings. The rolling direction (RD) is aligned along the x-direction. Both sheets are symmetrically meshed by hexahedral elements without the need for remeshing (based on [10]).*

Results. We study the influence of plastic orthotropy by analysing its effect on the overall sheet deformation, the characteristic parameters (interlock $i$, neck thickness $n$, shown in Fig. 3) and the process force. The sheet contours of the yz-plane (normal to x-axis, red, 90°, TD) and xz-plane (normal to y-axis, green, 0°, RD) for selected models are shown in the following.

For isotropic von Mises plasticity, the sheet contours from both planes match well and are shown as black reference contours in Fig. 3 and 4. Thus, the 3D model with isotropic plasticity is indeed symmetric. The geometric parameters, depicted in Fig. 5, confirm this symmetry.

Hill48-r obtains a slightly asymmetric deformation mainly visible by a higher interlock in rolling direction (green) in Fig. 3. This might be similar to the flow behaviour observable in the layer compression test, where the material flow is less pronounced in rolling direction. The higher interlock is compensated by a thinner neck in rolling direction, as summarised in Fig. 5. Moreover, the asymmetry and difference to isotropic plasticity (black) can also be seen in the upper corner A in Fig. 3, where Hill48-r predicts less vertical flow into the joint.

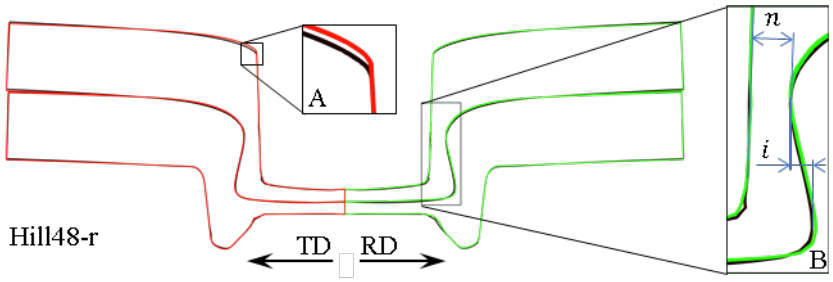


*Fig. 3. Hill48-r. Sheet contours of the clinched joint. A small asymmetry is visible for the interlock in TD (red) and RD (green). Moreover, also the vertical flow into the joint (zoom A) is affected by anisotropy compared to the isotropic model (black). The zoom window B shows the definition of the interlock $i$ and neck thickness $n$.*

Hill48-rn well represents the symmetry in in-plane direction, thus is not shown in detail, but only summarised in Fig. 5. Hill48-s renders only a small asymmetry in the deformation, thus is also not shown in detail and is on average similar to Hill48-r, see Fig. 5.

Hill48-rs in Fig. 4 predicts a larger asymmetry of the interlock and neck thickness than the previous models, however with ratios $i_{RD}/i_{TD} = 1.07$ and $n_{RD}/n_{TD} = 0.96$ still relatively low and within the experimental scatter indicated in Fig. 5 by the shaded areas.

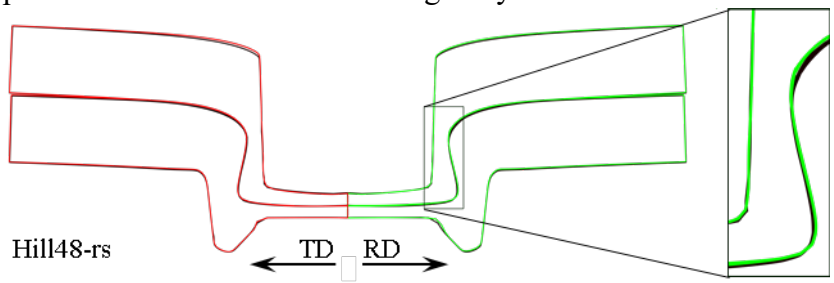


*Fig. 4. Hill48-rs. Sheet contours of the clinched joint. The asymmetry between rolling (RD, green) and transverse direction (TD, red) is more pronounced visible by a larger interlock and thinner neck in rolling direction (green, zoom window).*

The interlock $i$ and neck thickness $n$ are extracted from the numerical results as shown in Fig. 3 (right) and summarised in Fig. 5. All anisotropy models show in rolling direction a higher interlock and a thinner or almost equal neck thickness. The non-associative model Hill48-rs exhibits the highest geometric asymmetry, where it appears to combine the results for Hill48-r and -s. Thus, it appears to be important to capture both anisotropy effects. Nevertheless, in view of the experimental scatter, the asymmetry is negligible, so the in-plane anisotropy could be omitted. Moreover, the anisotropy does not only relocate the material between rolling and transverse direction, but also increases the interlock overall. This might be accounted to the changing flow behaviour that is introduced by the r-values. The Hill48-rn renders a nearly symmetric deformation with a higher interlock than the von Mises model and a slightly lower neck thickness. This confirms that the anisotropy in sheet thickness direction already notably influences the characteristic parameters and further supports the use of a 3D anisotropy model.

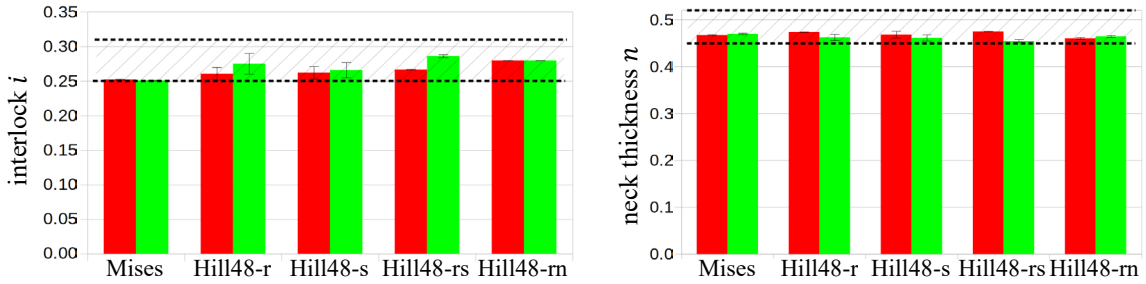


*Fig. 5. Comparison of interlock (left) and neck thickness (right) for all models. Red: transverse direction (TD). Green: rolling direction (RD). The shaded areas with dashed upper and lower bounds indicate the experimental range. Anisotropy relocates the material between RD and TD and moreover increases the interlock.*

Further analysis shows a continuous transition of these results between rolling and transverse direction. Thus, the extrema are well captured by considering only the yz- and xz-planes as depicted in the figures and diagrams above. Also changing the relative orientation of the die-sided and punch-sided sheet revealed no different trends.

The comparison of the process force for all models shows no clear tendency in Fig. 6 (left) as all match the experimental results (black) well. All forces evolve similarly with a certain scatter mainly due to unsmooth changes in the contact states. The process force seems to be dominated by the compression of the two sheets between the punch and the die, which is governed by the

flow stress in sheet thickness direction being equal for all models. Fig. 6 (right) confirms that the joint contours for von Mises (blue) as well as Hill48-rs (red) match well to experiments (black).

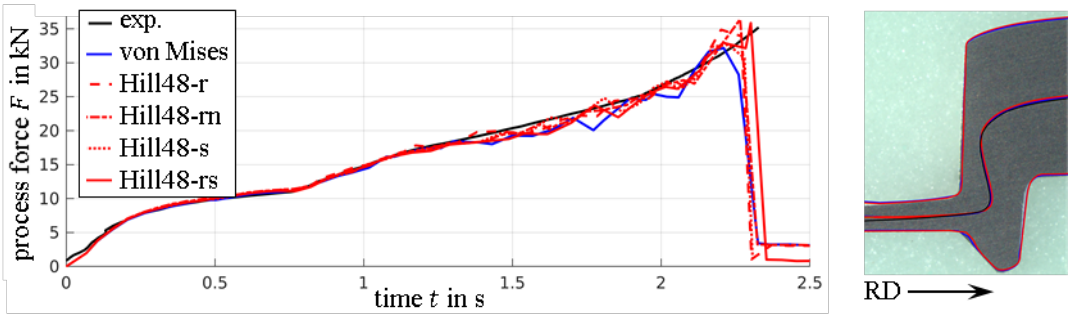


*Fig. 6. Process force vs process time for different material models (left). All models match the experimental result (black) well. The different anisotropy models show no clear trend, such that the process force is rather independent and mainly affected by the flow stress in sheet thickness direction. The simulated joint contours for von Mises (blue) and Hill48-rs (red) plasticity match well to the experimental results (black).*

## Summary and Outlook

We implemented different 3D anisotropic plasticity models in LS-Dyna for the simulation of 3D clinching. The goal was to set up robust material and simulation models to study the influence of plastic orthotropy on the clinching process. Thereby, we compared different variants of the Hill48 yield function including associative and non-associative flow rules being equipped with different experimental input. The shown results are confined to an aluminium alloy EN AW-6014 T4, which revealed only a minor influence and asymmetry of geometric and process parameters due to plastic orthotropy. However, it was shown that the anisotropy between in-plane and sheet thickness direction can alone notably affect the clinched joint. Moreover, the use of a non-associative plasticity model that accurately captures more features of the sheet orthotropy led to a more pronounced asymmetry, however still well within experimental scatter. Even though the non-associative model is therefore recommended for higher predictability, it is seen as more important to accurately capture the ratio between in-plane and out-of-plane plastic flow. Especially for aluminium alloys a non-quadratic yield function is necessary, for instance Yld91, which however possesses the same anisotropy properties as the herein applied Hill48 model. This work lays the basis for a parametric study on the influence of advanced plasticity characteristics to understand when certain phenomena are relevant for reliable and versatile clinching of sheet metal. To quantify the effect of the geometric changes on the joint strength, for instance pull-out tests can be utilised in future work as part of a continuous simulation chain.

## Acknowledgements

The funding by the Deutsche Forschungsgemeinschaft (DFG, German Research Foundation) – Project-ID 418701707 – TRR 285, subproject A01 and A05 is gratefully acknowledged. Moreover, we want to thank our colleagues in the TRR285 Lars Ewenz (B02) and Simon Wituschek (C02) for their support.

## References

[1] M. Jäckel et al., Process-oriented flow curve determination at mechanical joining, Procedia Manufacturing, 47 (2020) 368-374. https://doi.org/10.1016/j.promfg.2020.04.289

[2] M. Böhnke, F. Kappe, M. Bobbert, G. Meschut, Influence of various procedures for the determination of flow curves on the predictive accuracy of numerical simulations for mechanical joining processes, Materials Testing, 63(6) (2021) 493-500. https://doi.org/10.1515/mt-2020-0082

[3] S. Saberi et al., Influence of plastic anisotropy on the mechanical behavior of clinched joint of different coated thin steel sheets. Int. J. Mater. Form. 1(1) (2008) 273-276. https://doi.org/10.1007/s12289-008-0349-9

[4] S. Coppieters et al., Numerical and experimental study of the multi-axial quasi-static strength of clinched connections. Int. J. Mater. Form. 6(4) (2013) 437-451. https://doi.org/10.1007/s12289-012-1097-4

[5] R. Hill, A theory of the yielding and plastic flow of anisotropic metals, Proc. R. Soc. Lond. 193(1033) (1948) 281-297. https://doi.org/10.1098/rspa.1948.0045

[6] A. Breda, S. Coppieters, T. Kuwabara, D. Debruyne, The effect of plastic anisotropy on the calibration of an equivalent model for clinched connections. Thin-Walled Structures, 145 (2019) 106360. https://doi.org/10.1016/j.tws.2019.106360

[7] S. Coppieters et al., Reproducing the experimental pull-out and shear strength of clinched sheet metal connections using FEA. Int. J. Mater. Form. 4(4) (2011) 429-440. https://doi.org/10.1007/s12289-010-1023-6

[8] S. Jónás, M. Tisza, Finite element modelling of clinched joints, Adv. Technol. Mater. 43(1) (2018) 1-6. https://doi.org/10.24867/ATM-2018-1-001

[9] J. Friedlein et al., Inverse parameter identification of an anisotropic plasticity model for sheet metal. In IOP Conference Series: Mater. Sci. Eng. 1157(1) (2021) 012004. https://doi.org/10.1088/1757-899X/1157/1/012004

[10] C.R. Bielak, M. Böhnke, M. Bobbert, G. Meschut, Numerical investigation of a friction test to determine the friction coefficients for the clinching process. Proc. Inst. Mech. Eng. L: Journal of Materials: Design and Applications, 14644207221093468 (2022).

[11] C. Miehe, N. Apel, M. Lambrecht, Anisotropic additive plasticity in the logarithmic strain space: Modular kinematic formulation and implementation based on incremental minimization principles for standard materials, Comput. Methods Appl. Mech. Engrg. 191(47-48) (2002) 5383–5425. https://doi.org/10.1177/14644207221093468

[12] T.B. Stoughton, A non-associated flow rule for sheet metal forming. Int. J. Plast. 18(5-6) (2002) 687-714. https://doi.org/10.1016/S0749-6419(01)00053-5

[13] J.C. Simo, T.J.R. Hughes, Computational inelasticity, 7, Springer Science & Business Media, 2006.

[14] A.M. Habraken, Modelling the plastic anisotropy of metals. Arch. Comput. Methods Eng. 11(1) (2004) 3-96. https://doi.org/10.1007/BF02736210

[15] O. Ghorbel et al., Coupled anisotropic plasticity-ductile damage: Modeling, experimental verification, and application to sheet metal forming simulation. Int. J. Mech. Sci. 150 (2019) 548-560. https://doi.org/10.1016/j.ijmecsci.2018.10.044

[16] P. Dasappa, K. Inal, R. Mishra, The effects of anisotropic yield functions and their material parameters on prediction of forming limit diagrams. Int. J. Solids. Struct. 49(25) (2012) 3528-3550. https://doi.org/10.1016/j.ijsolstr.2012.04.021